Breast Mass Segmentation via Enhanced U-Net++ Using Gradient and Contrast Information Reconstruction

Miao Guo[1, *], Ating Yang[2], Min Dong[2, 3]
[1]Zhengzhou Technical College, Xingyang ,Zhengzhou 450010, China
[2]School of Electrical and Information Engineering, Zhengzhou University ,Zhengzhou, 450001, China
[3]Industrial Technology Research Institute, Zhengzhou University, Zhengzhou, 450001, China
E-mail: guomiao12@126.com
[*]Corresponding author

Keywords: mass segmentation, mammogram images, image enhancement, U-net++

Received: March 4, 2025

This study introduces an innovative image enhancement technique to enhance breast mass segmentation in mammograms, where edge gradients are frequently feeble and concealed by adjacent tissues. The method combines gradient and contrast information reconstruction to improve essential structural aspects. Gradient reconstruction utilizes a total variation-based model integrated with Haar wavelet transform (HWT), efficiently attenuating high-frequency noise while retaining low-frequency structural details crucial for accurate mass boundaries. Edge features are obtained via the Scharr operator and enhanced through K-Singular Value Decomposition (K-SVD) dictionary learning, which develops adaptive basis functions to denoise and sharpen mass edges. Structural and edge reconstructions are linearly combined with weights of 0.7 and 0.3, respectively, resulting in improved images. The enhanced images are segmented utilizing a U-Net++ architecture, trained with a learning rate of 0.001, a batch size of 4, and the Adam optimizer, incorporating fivefold cross-validation for a thorough assessment. Experiments were performed on 60 mammographic images from the DDSM-BCRP subset, expanded to 360 samples. The proposed method attained a Dice coefficient of 96.52%, an IoU of 93.30%, a sensitivity of 96.56%, and an accuracy of 98.84%, surpassing baseline models. The enhanced segmentation enables more precise lesion localization within Computer-Aided Diagnosis (CAD) systems, thereby aiding in the early detection of breast cancer. Currently, validation is constrained to a modest dataset; subsequent efforts will aim to broaden the methodology to encompass larger, multi-institutional datasets to improve generalization.

Povzetek: Opisan je izboljšan algoritem U-Net++ z rekonstrukcijo gradienta in kontrasta za natančnejšo segmentacijo prsnih mas na mamogramih, s čimer bistveno izboljša natančnost CAD sistemov.

1 Introduction

Breast cancer continues to be one of the most fatal diseases affecting women globally, with mammography utilizing molybdenum target imaging as a primary screening method. Accurate mass segmentation is hindered by acquisition errors, tissue overlap, and scattering noise that conceal lesion boundaries. Diagnostic variability resulting from disparities in radiologists' expertise and human visual perception, including challenges in identifying small contrasts, exacerbates segmentation difficulties. Contemporary techniques frequently necessitate manual involvement and are only partially automated, constraining real-time application. Consequently, the integration of advanced segmentation approaches with Computer-Aided Diagnosis (CAD) systems has emerged as a pivotal objective to enhance the efficiency and reliability of mass detection for early breast cancer diagnosis.

In the present up-to-date practice, two primary medical image segmentation (MIS) methodologies are widely used: traditional ones and deep learning (DL) approaches. Traditional groups mainly include typical edge detection [1–3], region growing [4], and fuzzy clustering algorithms [5–7]. These methods generally have simple operations and perform well on simple images, but they often only consider a single grayscale factor. For molybdenum target images with uneven grayscale distribution, the segmentation performance of traditional methods is unsatisfactory. Recently, the U-Net++ network [8] has demonstrated remarkable segmentation performance in medical imaging, including brain tumors and pulmonary nodules, by improving feature fusion via restructured skip connections and dense blocks. This framework facilitates the adaptive incorporation of intricate features and overarching context, enhancing boundary precision. This work employs U-Net++ for breast mass segmentation in molybdenum target mammograms, using these characteristics. In mammographic pictures, the border gradients of breast masses frequently demonstrate weakness and exhibit low contrast compared to adjacent glandular and adipose tissues. The amalgamation of intensity profiles renders the mass edges visually indistinguishable from neighboring areas, complicating precise border detection and segmentation for traditional techniques. Utilizing low-quality images characterized by inadequate clarity and contrast for training may hinder the network's ability to discern precise boundaries, leading to incomplete segmentation and diminished accuracy.

Efficient image enhancement and network selection are crucial for optimizing breast mass segmentation in molybdenum target mammograms by more effectively delineating lesion boundaries, forms, and textures. This article presents an enhancement approach that integrates gradient reconstruction with contrast enhancement, subsequently employing a U-Net++ network for segmentation. Comparative tests were performed utilizing four datasets: original images, gradient-enhanced images, contrast-enhanced images, and photos altered with recognized enhancement techniques. Performance was assessed with the Dice coefficient, Intersection over Union (IoU), sensitivity, and accuracy. Additionally, relative studies use the suggested enhancement approach and the U-Net and U-Net++ networks. Visual analysis and impartial assessment of the SRs demonstrate that the technique suggested in this work, when applied to the U-Net++ network, exhibits superior segmentation performance compared to the unprocessed dataset and outperforms current advanced segmentation networks.

Progress in artificial intelligence (AI) has markedly enhanced pattern recognition tasks such as semantic segmentation [9,10], facilitating accurate item delineation in intricate images. Deep learning (DL) models are particularly adept at breast mass segmentation due to their automatic feature learning and structural representation, which improve boundary and texture detection.

1.1 Literature review

Oliveira et al. [11] assessed U-Net and U-Net++ for segmenting breast tumors in ultrasound images utilizing the BUSI dataset. Both models were trained for 1000 epochs utilizing data augmentation and an IoU-based loss function. U-Net++ surpassed U-Net, with a Dice score of 75.71% on validation data, 88.60% on test data, and an F1-score of 94% in tumor classification. The authors proposed enhancing performance by utilizing larger datasets and optimizing hyperparameters. Wisaeng [12] presented U-Net++DSM, a brain tumor segmentation technique that integrates U-Net++ with deep supervision and a dilation operator, demonstrating robust performance on constrained MRI data. Evaluated using public datasets, it surpassed conventional U-Net and other methodologies, achieving a 98.02% Dice score, 98.64% accuracy, and above 98% sensitivity and specificity, so illustrating its efficacy in pixel-level categorization. Tiryaki [13] proposed a cascaded deep transfer learning methodology for the segmentation and classification of breast masses utilizing mammograms. The U-Net++ model with an Xception encoder attained a Dice score of 0.6356, an IoU of 0.5408, and an AUC of 0.7829 for segmentation, along with an AUC of 0.8188 and an accuracy of 76.19% for classification, demonstrating its potential to aid diagnosis in the absence of clinical data. Ronneberger et al. [14] introduced U-Net, characterized by a symmetric "U"-shaped encoder-decoder architecture that integrates low-level spatial and high-level semantic data via skip links. Despite being a traditional model for medical image segmentation (MIS), U-Net's inflexible feature fusion frequently results in redundant learning and elevated training expenses. Zhou et al. [8] introduced the U-Net++ architecture, an enhancement of U-Net that incorporates several stacked U-Nets at varying depths. U-Net++ reconfigures skip connections by incorporating intermediary dense convolutional layers between the encoder and decoder, facilitating more adaptable and gradual feature fusion. It employs model pruning during training to eliminate redundant neural pathways, thereby decreasing network complexity and enhancing inference speed without compromising segmentation accuracy. Zhou et al. [15] proposed ATFE-Net to improve long-range dependency capture and feature integration for breast mass segmentation. By enhancing global context understanding, ATFE-Net outperformed conventional local feature-based methods, achieving Dice coefficients of 82.46% on the BUSI dataset and 86.78% on the UDIAT dataset for large-scale mass segmentation. Malekmohammadi et al. [16] proposed a fully automatic 3-D ABUS breast mass segmentation by combining a tumor detection network with a Bidirectional Convolutional Long Short-Term Memory (Bi-ConvLSTM) and a segmentation network with a 2-D attentive UNet. The saliency maps and enhanced attention modules increased the precision, while the Convolutional Block Attention Module handled variations of mass size. It reached a Dice similarity index of 85.82% for 60 ABUS volumes. Yaqub et al. [17] have suggested a DL concept for the diagnosis of breast cancer utilizing mammogram images, where segmentation is by Attention-Constrained Adaptive Atrous U-Net (ACA-ATRUNet), and classification is done by Attention-Constrained Adaptive-Multidimensional Network (ACA-AMDN). The proposed framework has segmented and classified the breast masses effectively while optimized by the Multi-Model Learning Optimization for Enhanced Output Optimization (MML-EOO) algorithm, showing superior performance that could enhance mammogram-based cancer screening. Rahman et al. [18] established a ResNet-50 framework utilizing transfer learning to classify INbreast mammograms as benign or malignant, achieving 93% precision. Deep learning (DL) enhances diagnostic precision by autonomously extracting nuanced image characteristics, facilitating early breast cancer identification and augmenting the dependability of computer-aided detection (CAD) systems. Mahmood et al. [19] created a Convolutional Neural Network (CNN) that attained 0.97 test accuracy, 0.99 sensitivity, 0.98 training accuracy, and 0.99 Area Under the Curve (AUC) for accurately classifying breast masses in mammograms. The model facilitates quicker treatment planning and diagnosis by utilizing improved data augmentation, transfer learning, and preprocessing on private and Mammographic Image Analysis Society (MIAS) datasets. Almalki et al. [20] introduced an image enhancement scheme to mammograms, including a step on low contrast and background noise suppression by Principal Component Analysis (PCA), morphological processing, and coherence enhancement with LoG and diffusion filters. The method was evaluated on 11,194 images, where an improved peak signal-to-noise ratio, difference, and Enhancement Measure Estimation (EME) were reported compared to previous approaches, thus improving diagnostic accuracy. Avcı and Karakaya [21] studied the effect of different preprocessing algorithms on the mammography image quality for CAD systems. They proposed a methodology based on the mini-MIAS database: a mixture of median filtering, Contrast Limited Adaptive Histogram Equalization (CLAHE), and unsharp masking (USM) for increasing resolution and visibility; suspicious region extraction by k-means; and classification of lesions by different machine learning approaches. The combination of MF with USM and CLAHE enhanced the accuracy, while the best performances were obtained by Support Vector Machine (SVM), RF, and NNs. This study proved that proper preprocessing is important to differentiate between benign and malignant lesions. Aliniya et al. [22] proposed a hybrid loss function to segment breast cancer, designed to handle pixel class imbalance and mass diversity difficulties. Their method outperformed various up-to-date techniques on a curated breast imaging subset of DDSM and INbreast. This had been in response to the incorporation of mass size and density within both sample-level and region-level loss calculations. Tiryaki [23] introduced cascaded deep transfer learning techniques for mammographic mass segmentation and classification based on the Breast Cancer Digital Repository dataset. The best-performing model was the Unet++ model with an Xception encoder, providing an AUC of 0.7829, a Dice coefficient of 0.6356, and an IoU of 0.5408 for segmentation tasks. Conversely, classification resulted in an AUC of 0.8188 and a precision rate of 76.19% from this model. Hence, the method showed its good promise in the automation of diagnosing breast cancer and alleviating the workload of radiologists.

Wisaeng [24] designed U-Net++DSM, which adds a Deep Supervision Mechanism and a dilation operator to U-Net++. This work used these modifications for brain tumor segmentation. That model provides the following performances: 98.59% sensitivity, 98.64% specificity, 98.64% accuracy, and a 98.02% Dice score. Das et al. [25] suggested a weighted U-Net++ model (WU-Net++) as a DL framework for segmenting brain tumors. This network has been tested on the BraTS 2018 dataset and yielded a Dice score of 0.91 and an AUC of 0.915. It also performed very well in intracranial hemorrhage classification with an accuracy of 0.9949 and multi-organ segmentation, showing its potential in precision medicine. Tambe-Jagtap and Jaaz [26] revealed that genetic and proteomic profiling can improve breast cancer treatment through the facilitation of tailored therapies. Focusing on abnormalities such as TP53 and BRCA1/2 resulted in a 60% reduction in tumors and diminished adverse effects relative to conventional therapies, underscoring the significance of personalized strategies. Houby [27] examined how trends such as transfer learning, active learning, and federated learning augment deep learning in medical imaging by mitigating data constraints, enhancing efficiency, and safeguarding privacy. These methodologies have demonstrated significant potential in recent publications in leading ScienceDirect journals. Shangguan et al. [28] presented ICU-Net, a denoising model for low-dose CT images that employs enhanced ConvNext blocks and attention mechanisms. Utilizing a blended loss to avert over-smoothing, ICU-Net attained enhanced PSNR, SSIM, and RMSE metrics, surpassing current methodologies while maintaining texture fidelity. Chegireddy and Srinagesh [29] created a deep learning framework for the early identification of pancreatic cancer with CPTAC-PDA data. The approach integrated U-Net++ segmentation, HHO-based CNN, and BOVW for feature extraction and selection, alongside VGG16 for classification, attaining an accuracy of 0.96 and surpassing other models.

Notwithstanding the progress of state-of-the-art segmentation networks such as Mask R-CNN, DeepLab, and ACA-ATRUNet, certain restrictions endure. Numerous models encounter difficulties in maintaining border integrity in low-contrast mammograms and demonstrate susceptibility to noise, particularly in thick breast tissues. Moreover, conventional networks are frequently trained on unprocessed pictures, which constrains their efficacy in the presence of gradient transitions or ambiguous lesion boundaries. Our approach directly tackles these challenges by augmenting contrast and structural clarity before segmentation, leading to substantial enhancements in Dice and IoU measures. In response to the reviewer's comments, we meticulously examined the listed references and eliminated those irrelevant to breast mass segmentation or image enhancement in mammographic imaging, so ensuring that all references now closely align with the study's objectives.

Table 1: Comparison of State-of-the-Art Breast Mass Segmentation Methods

Model	Dataset	Dice (%)	IoU (%)	Sensitivity (%)	Accuracy (%)	Reference
U-Net	BUSI	75.17	–	–	–	Oliveira et al. [11]
U-Net++	BUSI	88.60	–	–	90.00	Oliveira et al. [11]
U-Net++DSM	Brain MRI	98.02	–	98.59	98.64	Wisaeng [12][24]
U-Net++ + Xception	BCDR	63.56	54.08	–	76.19	Tiryaki [13][23]
ATFE-Net	BUSI / UDIAT	82.46	–	–	–	Zhou et al. [15]
DeepLabV3+	Private	90.20	82.70	91.50	95.10	Das et al. [25]

ACA-ATRUNet (segmentation)	Mammogram	–	–	–	–	Yaqub et al. [17]
Proposed Method (this work	DDSM	96.52	93.30	96.56	98.84	–

1.2 Research gaps and novelties

This research tackles significant obstacles in breast mass segmentation through mammography by surmounting the shortcomings of conventional and deep-learning methodologies. Traditional techniques, such as edge identification and fuzzy grouping, exhibit suboptimal performance due to the dispersion of grayscale values and indistinct edges resulting from tissue overlap, insufficient lesion contrast, and image noise. Despite advancements in segmentation through deep learning models such as U-Net++, challenges persist with gradual gradient transitions at lesion boundaries and interference from heterogeneous adjacent tissues, especially under conditions of low image quality.

Numerous research persists in the use of unprocessed mammograms, wherein inadequate clarity further diminishes segmentation precision. Recent research underscores the imperative for sophisticated preprocessing methods to improve input quality and maximize the efficacy of deep learning models. This paper proposes an image enhancement technique utilizing Haar wavelet transform (HWT) and K-Singular Value Decomposition (K-SVD) to mitigate noise, sharpen edges, and enhance contrast. Enhanced pictures are segmented with a U-Net++ network with fivefold cross-validation, resulting in a Dice coefficient of 96.52% and an IoU of 93.30%. Comparative trials with alternative enhancement approaches validate the efficacy of the suggested technique in enhancing breast cancer diagnosis and broader medical imaging applications.

To direct this inquiry, we establish the subsequent research questions:

How can gradient and contrast information be utilized to enhance mammographic image quality for deep learning segmentation?

Does the incorporation of augmented picture inputs into U-Net++ enhance segmentation performance compared to standard inputs or single-mode enhancement?

What is the ideal fusion approach for structural and edge-based image components to enhance segmentation accuracy?

1.3 Paper organization

The document is defined in the way as follows: Section 2 explains the aspects of the proposed enhanced image algorithm focusing on gradient and contrast information, reconstruction for better clarity and boundary definition in mammograms, and integration into the U-Net++ network within the framework of five-fold cross-validation. Section 3 provides a detailed explanation of the empirical setup and findings: a dataset and the pre-processing step to show the proposed methodology vis-a-vis all the methods applied herein. In addition, a deeper scrutiny of its effectiveness in light of metrics such as segmentation accuracy, sensitivity, robustness, and generalizability are carried out by comparing the different network performances. Section 4 summarizes the results obtained from this investigation, which are related to the segmentation of breast masses through the proposed methodology, further discussing possible directions for future research on medical images by processing and segmentation.

2 The method for mammographic mass segmentation by fusing gradient and contrast information reconstruction

Segmentation of breast masses presents difficulties owing to the gradual intensity changes at mass boundaries and the poor contrast between lesions and adjacent tissues, which obscure edge delineation and hinder the precise localization of mass margins by both classical and deep learning models. This study presents a segmentation method utilizing the U-Net++ network, augmented by a gradient and contrast information reconstruction process to improve image quality before segmentation. As illustrated in Fig. 1, the method initially reconstructs the gradient information of the mammography to emphasize structural boundaries, thereafter using contrast enhancement to augment the differentiation between masses and surrounding tissues. The amalgamated gradient and contrast data are integrated to produce an upgraded image featuring more defined mass edges and superior lesion-background differentiation. The improved image is subsequently utilized as input for the U-Net++ network, which is trained inside a fivefold cross-validation framework to effectively segment breast masses. Every stage in the flowchart signifies a crucial improvement or segmentation phase aimed at resolving particular imaging challenges. The suggested image enhancement framework amalgamates gradient and contrast data to enhance mammographic mass segmentation. A total variation model is employed for gradient reconstruction to recover structural components and attenuate high-frequency noise while maintaining the integrity of the underlying tissue architecture. Edge enhancement is accomplished through the application of the Scharr operator for fine boundary detection, succeeded by K-SVD dictionary learning for the reconstruction and denoising of edge details. The structural image is deconstructed by the Haar Wavelet Transform (HWT) to distinguish low- and high-frequency subbands for contrast reconstruction. A gamma correction function is utilized on the deconstructed components to adaptively boost contrast, and the altered subbands are recombined to produce the contrast-enhanced image. The gradient- and contrast-enhanced outputs are linearly combined using empirically established weights (0.7 for structure and 0.3 for edge) to provide the final input image for U-Net++ segmentation. These measures guarantee the preservation and optimization of both edge precision and tissue contrast for subsequent deep-learning efficacy.

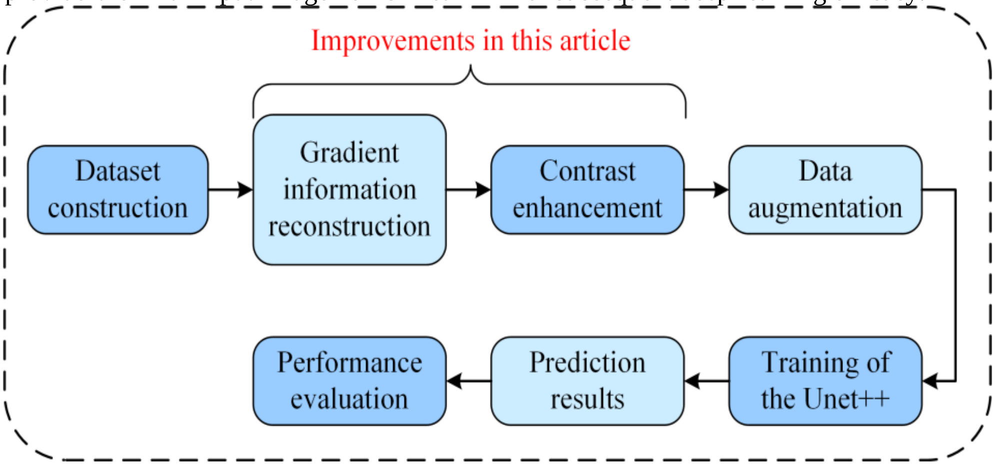

Figure 1: Experimental flow chart

2.1 The Method for Enhancing Masses by Fusing Gradient and Contrast Information Reconstruction

2.1.1 Reconstruction of gradient information

A total variation-based model was utilized to extract the structural components of mammographic pictures due to its adaptability in differentiating structural and textural information without dependence on predetermined texture assumptions. This model employs terms such as $H_x(p)$, $K_x(p)$, and the Gaussian weighting function gp,q to delineate local spatial fluctuations and facilitate precise structure extraction. The regularization parameter λ governs smoothness, with values ranging from 0.01 to 0.03 selected to equilibrate noise reduction and feature preservation. A universal window-based total variation metric H facilitates adaptation across diverse tissue patterns. In Haar wavelet transform (HWT) processing, the low-frequency (LF) subband of the original image is utilized to substitute that of the structure image, thereby reducing information loss caused by pixel averaging. The Scharr operator is favored over the Sobel operator for edge detection due to its superior gradient sensitivity and enhanced border localization. K-SVD dictionary learning improves edge reconstruction by considering each column in the sample matrix Y as a vectorized image patch for sparse representation and denoising. Ultimately, structural and edge pictures are combined using linear weighting (0.7 for structure, 0.3 for edges) derived from experimental optimization, resulting in an enhanced image with more distinct lesion characteristics, as illustrated in Fig. 1.

(1) Extraction of image structural components based on the total variation from the model [30]. In structural component extraction, a model based on the total variation form is used, which can reasonably analyze the structure and texture information of the image without specifying particular texture rules. The model can be represented as:

$$\arg\min_{S} \sum_{p} (S_p - I_p)^2 + \lambda \cdot \left(\frac{H_x(p)}{K_x(p)+\varepsilon} + \frac{H_y(p)}{K_y(p)+\varepsilon} \right) \tag{1}$$

$$H_x(p) = \sum_{q\in R(p)} g_{p,q} \cdot \left|(\partial_x S)_q\right| \tag{2}$$

$$H_y(p) = \sum_{q\in R(p)} g_{p,q} \cdot \left|(\partial_y S)_q\right| \tag{3}$$

$$K_x(p) = \left| \sum_{q\in R(p)} g_{p,q} \cdot (\partial_x S)_q \right| \tag{4}$$

$$K_y(p) = \left| \sum_{q\in R(p)} g_{p,q} \cdot (\partial_y S)_q \right| \tag{5}$$

Where (I) signifies the input image, (p) denotes the index value of 2D image pixels, (O) signifies the output structural image, (q) denotes the pixel index within a square range centered at (p), fixed at 0.001 to prevent division by zero, (λ) is the weight used to adjust the smoothness of the image, generally set between 0.01 and 0.03, the empirical value of the spatial scale parameter is between 0 and 8, which limits the size of the window in formulas (1) to (5), playing a crucial role in the structural extraction process, and (K) represents the Gaussian kernel function, which can be expressed as:

$$g_{p,q} \propto \exp\left(-\frac{(x_p - x_q)^2 + (y_p - y_q)^2}{2\sigma^2} \right) \tag{6}$$

Due to the diverse texture types in different images, the algorithm does not assume or artificially determine the texture type beforehand. Instead, it adopts a universal pixelized window total variation measure H, where $H_x(p)$and $H_y(p)$ respectively represent the windowed total changes in the x and y directions of the pixels utilized to calculate the absolute spatial differences within the window. $K_x(p)$ and $K_y(p)$ is a new windowed inherent variation utilized to assist in separating the texture from the main structures. This step extracts the structural part of the molybdenum target image, removes high-frequency information (HFI), and retains only the original image's low-frequency information (LFI) utilized for the following rebuilding of LFI.

(2) Image structure reconstruction based on the HWT. The rebuilding of the structural part of the breast molybdenum target image is carried out using the HWT. The HWT extracts the breast structure image's LF subband and three HF subbands. Since the structural image has already lost some information compared to the original image, and when extracting the LF subband using the HWT, a "mean" method is applied to compress the number of pixels, resulting in a lower-resolution image. This means that this subband has lost some information, so the LF subband of the structural image is discarded. The LF subband obtained by performing the HWT on the original image is used to replace the LF subband of the structural image, and wavelet reconstruction is conducted with the three HF subbands of the structural image. The LF subband of the original image contains rich LFI, while the three HF subbands contain the singular characteristics of the LFI. This avoids the problem of dimension mismatch between subbands during wavelet reconstruction and maximizes the preservation of the LFI of the image.

(3) Extraction of image edge parts based on gradient operators. The edge part of the image is the most critical HFI in the molybdenum target image, and this HFI is vital in the subsequent segmentation of tumor edges. An edge is the endpoint of one region and the starting point of another area, so the grayscale information at the edge has abrupt changes. Objects and backgrounds can be segmented based on this characteristic. This study mainly uses the Scharr operator to extract the edge information of tumors. Compared to the commonly used Sobel operator, the Scharr operator, with the same computational complexity and speed, has different convolution kernel coefficients. The Scharr operator is more sensitive in extracting edge localization information than the Sobel operator and can capture finer boundary information. It succeeds in isolating the HFI from the image. In that sense, the process provides the grounds for further gradient reconstruction of edge images.

(4) Image edge reconstruction based on K-SVD learning. The method utilizes K-SVD dictionary learning to train the dictionary for extracting the edge part of the breast image. This step is known as "sparse coding" to learn the dictionary D during the training phase. From the basic matrix analysis theory, sample Y should be viewed as a matrix, where each column represents a set of samples. The Y matrix is decomposed into D and X matrices through dictionary learning. This process can be represented by formula (7).

$$Y \approx D * X \tag{7}$$

Where D represents the dictionary structure, each column of D is called an atom, and X represents the encoding vector. Every column of D is a normalized vector, and X should be as sparse as feasible. The objective function of dictionary learning is:

$$D、X = \begin{cases} \underset{D、X}{argmin}\|Y - DX\| \\ \|X\|_0 \leq L \end{cases} \tag{8}$$

The parameter L is the sparsity constraint parameter. Since the objective function involves two unknown variables, this algorithm's solution process involves fixing one variable, updating the other variable, and then updating them alternately.

This paper uses sparse coding to denoise breast edge images. Since breast edge images are composed of noise-free and noisy images, sparse operations can be performed on the original noise-free images, expressed in the form of a finite number of "atoms." The noisy images are non-sparse, so the K-SVD dictionary training is utilized to extract the sparse components of the image, which are then reconstructed to attain the denoised image. This procedure reconstructs the HFI of the molybdenum target image, namely the reconstructed image of the breast lump edge.

(5) Linear weighting. In Eqs. (1) and (4), the reconstructed images of the breast structure and edge parts have been obtained. These two parts are linearly weighted. After multiple experiments, the weight of the structural reconstruction image is fixed at 0.7, and the weight of the edge reconstruction image is fixed at 0.3. Finally, the gradient information reconstructed image with more prominent lesion information is obtained. The final improved image is generated by integrating structural and edge reconstructions through a linear weighting technique, employing a ratio of 0.7 for structure and 0.3 for edge. The weighting was empirically determined by assessing segmentation performance (Dice and IoU) across several configurations; the 0.7:0.3 ratio consistently provided the optimal compromise between maintaining anatomical boundaries and reducing noise. K-SVD dictionary learning was utilized for edge enhancement, employing a dictionary including 256 atoms, a patch size of 8×8 pixels, and a sparsity constraint permitting a maximum of 5 non-zero coefficients per patch. The parameters were optimized to accurately capture high-frequency edge structures while minimizing noise. During the contrast reconstruction step, gamma correction was implemented with a gamma value of 4. This value was selected after assessing several gamma values, with $\gamma = 4$ providing optimal visual augmentation of low-intensity areas without oversaturation and enhancing segmentation uniformity in first trials. These configurations were tuned to provide efficient pre-processing before U-Net++ segmentation.

Input: Original mammographic image I
Output: Enhanced image I_enhanced
Step 1: Gradient Reconstruction
2. Extract structural component S from I using total variation (TV) model
3. Replace LF subband of S with that of I using Haar Wavelet Transform (HWT)
4. Apply Scharr operator to I for edge detection → obtain edge map E
5. Apply K-SVD dictionary learning to E → denoised edge map E_denoised
6. Linearly combine S and E_denoised:

I_gradient = 0.7 * S + 0.3 * E_denoised
Step 2: Contrast Enhancement
8. Decompose I_gradient using HWT into LF and HF subbands
9. Apply gamma correction ($\gamma = 4$) to LF subband
10. Reconstruct contrast-enhanced image I_contrast using corrected LF and original HF subbands
11. Set I_enhanced ← I_contrast
12. Return I_enhanced

2.1.2 Contrast reconstruction

The operation in Section 1.1.1 can effectively reduce the noise around the mass, making the gradient of the mass boundary larger and, to some extent, overcoming the problem caused by the gradual change in the characteristics of breast lesion edges. However, because the difference between the lesion area and the surrounding glandular tissue in the mammographic image is not distinct enough, enhancing the contrast is particularly important. Applying the gamma transformation, it is easy to know that if $\gamma>1$, higher grayscale values of an image are stretched while the lower grayscale values are squeezed. In case $\gamma<1$, the lower grayscale values are stretched, and the higher grayscale values are squeezed. So, in this paper, γ is fixed as 4, which markedly increases the contrast between the mass and the surrounding area, and the mass becomes very clear. The suggested image enhancement architecture to address noise, edge gradients, and inadequate contrast to improve breast mass segmentation in mammograms is shown in Fig. 2. LF features are preserved. In contrast, the structural portion of the image is refined using wavelet reconstruction after being retrieved using a total variation-based model. The Scharr operator collects the edge information to reduce noise and define boundaries, which is then improved via K-SVD dictionary learning. The structural and edge components are linearly weighted (0.7 and 0.3) to create a gradient-enhanced image. The image is then subjected to gamma treatment ($\gamma=4$) to improve contrast and highlight the lesion. Breast mass visibility and segmentation accuracy are much increased by this method.

Fig. 2. Flowchart for the improvement of molybdenum target images via gradient and contrast reconstruction techniques. Initially, structural information is obtained by a total variation (TV) model and Haar wavelet transform (HWT). Edge information is augmented with the Scharr operator and subsequently denoised through K-SVD dictionary learning. Gradient and contrast data are recreated independently: gradient enhancement accentuates lesion borders, whilst contrast enhancement is executed by gamma transformation following wavelet decomposition. Structural and edge reconstructions are subsequently integrated via linear weighting to get an improved image with more distinct mass features for U-Net++ segmentation.

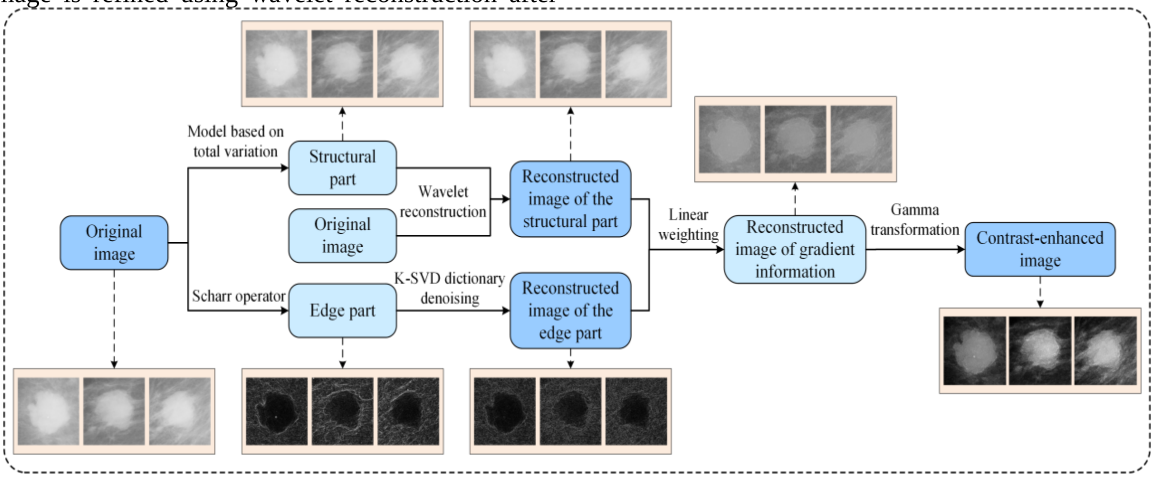

Figure 2: Molybdenum target image enhancement flow chart based on gradient information and contrast reconstruction

2.2 Breast Mass Segmentation Based on U-Net++

After enhancing the images using the method in Section 1.1, this study employs the U-Net++ network for breast mass segmentation. The U-Net++ network is an improvement based on the U-Net network, where features at each level are fully integrated using skip connections. During network training, the network autonomously learns features at different levels. This network adopts a nested structure, equivalent to concatenating four U-Net models of various depths. The U-Net substructures of different depths share a feature extractor, significantly reducing training time. Each U-Net sub-network output is supplemented with deep supervision, adding 11 convolutional kernels to detect the production of each U-Net sub-network. In the U-Net++ segmentation system, every intermediate decoder node is linked to a deep supervision branch to enhance gradient propagation and promote early feature refining. A convolutional layer is performed, followed by a 1×1 convolution operation, resulting in 11 feature maps. The convolutional kernels are initialized randomly and modified by backpropagation during the training process. The number 11 was empirically chosen to optimize the balance between segmentation detail acquisition and network complexity. Deep supervision across many semantic levels enhances the model's ability to generate more coherent and precise mass segmentations by directing intermediate representations towards the ultimate segmentation goal.

The outputs of each U-Net sub-network are not directly connected to the final output, allowing for model pruning and flexible selection of network depth through pruning operations. During training, the input images undergo forward propagation, and the pruned parts can assist in weight updates for the remaining parts during backpropagation. During testing, only forward propagation is performed on the input images, and the pruned parts have no impact on the output results, significantly reducing the parameter count and improving testing speed. Therefore, this study uses the U-Net++ network for breast mass segmentation.

3 Experimental Results and Analysis

3.1 Experimental Data and Experimental Settings

This experiment's breast molybdenum target image data is from the Breast Cancer Resistance Protein (BCRP) subset of the DDSM. For the 60 samples with prominent masses, the interested regions were cropped to obtain images with a size of 256x256 and a bit depth of 8 bits. Data augmentation was conducted on these 60 samples to avoid overfitting during training. The label images were annotated using LabelMe software, resulting in a total of 360 image samples and label samples. All experiments were performed on a workstation equipped with an NVIDIA RTX 3090 GPU (24 GB VRAM), 128 GB RAM, and an Intel Core i9 processor, operating on Ubuntu 20.04 with Python 3.9, TensorFlow 2.10, and Keras 2.7.

The experiment employed five-fold cross-validation to compare the SRs of datasets with various augmentation operations input into U-Net++. Four loss curves and objective evaluation metrics were provided for four different scenarios. The experiment set the learning rate to 0.001, each batch contained four training samples, the epoch was set to 100, and the model utilized the Adaptive Moment Estimation (ADAM) optimizer to dynamically adjust the update step size. The loss values were recorded during training, the best training model was saved, and this model was used for testing. Sixty mammography pictures featuring breast masses were extracted from the dataset. To prevent overfitting during training, data augmentation was implemented on these samples, incorporating random rotations between –15° and +15°, horizontal and vertical flips, scaling variations of ±10%, and minor brightness modifications. These augmentations augmented sample variety and improved model generalization.

The Adaptive Moment Estimation (Adam) optimizer was employed for model optimization, utilizing an initial learning rate of 0.001, with β_1 configured to 0.9 and β_2 to 0.999. Adam dynamically modifies the learning rate for each network parameter by assessing the first and second moments of gradients, promoting steady and efficient convergence throughout training. The U-Net++ network was trained using a batch size of 4, and fivefold cross-validation was conducted to enhance robustness and reduce bias in performance assessment. The learning rate of 0.001 and batch size of 4 were determined through initial experiments aimed at optimizing validation Dice scores. The Adam optimizer was selected for its demonstrated efficacy in training deep networks with moderate dataset sizes. No substantial improvements were noted with reduced learning rates or increased batch sizes. Five-fold cross-validation was selected to ensure statistical rigor and reduce overfitting, especially due to the limited sample size. This technique offers a dependable assessment of model generalization by guaranteeing that each sample is included in a test fold precisely once. Data augmentation was conducted on all 60 original photos through random rotation (±10 degrees), horizontal flipping, scaling (90–110%), and minor intensity variation. The modifications were uniformly implemented throughout all five folds to ensure consistency in the distribution of training and validation data. The linear fusion weights (0.7 for structural reconstruction and 0.3 for edge reconstruction) were experimentally determined after numerous attempts utilizing weight combinations from 0.1 to 0.9. The chosen ratio consistently produced the optimal segmentation metrics (Dice and IoU) across validation folds.

3.2 Evaluation Metrics

3.2.1 Image enhancement evaluation metrics

To make the enhanced effect of the image more intuitive, this paper uses two evaluation metrics, Spatial Frequency (SF) and Average Gradient (AG), to evaluate the image enhancement effect [31]. SF and AG are represented by Eqs. (9) and (12), respectively.

Spatial Frequency (SF) quantifies the overall detail and textural complexity present in an image. It illustrates the swift alterations in intensity across various sections of the image, including both horizontal and vertical fluctuations. A high SF value signifies that the image exhibits finer structural details and sharper transitions between various regions, leading to visibly cleaner edges and more complex texture patterns. A low SF value indicates that the image is smoother and morefuzzy, exhibiting diminished structural information and fewer well-defined boundaries. This study employs SF to statistically evaluate the efficacy of image enhancement techniques in preserving fine structures and enhancing mass visibility.

$$SF(I) = \sqrt{RF^2 + CF^2} \tag{9}$$

$$RF = \sqrt{\frac{1}{MN}\sum_{i=1}^{M-1}\sum_{j=1}^{N-1}\left(I(i,j) - I(i,j+1)\right)^2} \tag{10}$$

$$CF = \sqrt{\frac{1}{MN}\sum_{i=1}^{M-1}\sum_{j=1}^{N-1}\left(I(i,j) - I(i+1,j)\right)^2} \tag{11}$$

$$AG(I) = \frac{1}{(M-1)(N-1)}\sum_{i=1}^{M-1}\sum_{j=1}^{N-1}\sqrt{\frac{\left(I(i+1,j) - I(i,j)\right)^2 + \left(I(i,j+1) - I(i,j)\right)^2}{2}} \tag{12}$$

Here, I signifies the input image, RF signifies the row frequency, CF denotes the column frequency, and M and N denotes the height and width of the image. The SF of an image can also reflect the grayscale variation rate of the image. In an image, different components correspond to different spatial frequencies. For example, edges represent the highest SF of pixel detail information, while backgrounds represent lower spatial frequencies of large flat areas. Therefore, the higher the SF, the higher the visual clarity of the pixels and the more pronounced the detailed information content of the image. AG can also be an essential criterion for determining image clarity. Generally, the larger the AG, the higher the image clarity.

3.2.2 Image segmentation evaluation metrics

In medical image processing, to objectively and quantitatively analyze and evaluate SRs, people often compare the SRs of algorithms with labels at the same pixel level. The Average Gradient (AG) is a crucial metric for image sharpness, denoting the mean magnitude of intensity variations between neighboring pixels throughout the image. An elevated AG value indicates more abrupt intensity shifts, resulting in borders and boundaries within the image seeming more distinct and visually defined. A diminished AG value signifies more uniform intensity fluctuations, resulting in indistinct or poorly delineated edges. This study utilizes AG to assess the efficacy of enhancement techniques in refining image borders, highlighting distinct mass contours essential for precise segmentation. The metrics used in this article include IoU, Precision, Sensitivity, F1-Score (Dice Coefficient), Specificity, and Accuracy, defined as [32] :

$$IoU = \frac{TP}{FN + FP + TP} \tag{13}$$

$$Precision = \frac{TP}{TP + FP} \tag{14}$$

$$Sensitivity = \frac{TP}{TP + FN} \tag{15}$$

$$F1 - Score = \frac{2TP}{2TP + FP + FN} \tag{16}$$

$$Specificity = \frac{TN}{TN + FP} \tag{17}$$

$$Accuracy = \frac{TP + TN}{TP + TN + FP + FN} \tag{18}$$

Among them, TP (True Positive) represents true positives, where "True" indicates correct predictions, meaning the prediction is consistent with the actual situation, and "Positive" refers to positive or positive samples. FN (False Negative) signifies false negatives, where "False" indicates incorrect predictions, meaning the prediction is inconsistent with the actual situation, and "Negative" refers to negative or negative samples. Similarly, TN (True Negative) denotes true negatives, and FP (False Positive) signifies false positives.

IoU is the ratio between the intersection and union of the SR and the label. Precision, also known as Positive Predictive Value or Class Pixel Accuracy. Sensitivity, also referred to as Recall or TP Rate, represents the ratio of the SR to the label, reflecting the ability to identify pixels in the ROI. Meanwhile, the Dice coefficient represents the ratio of the intersection of two objects to the entire area in image segmentation problems. The mathematical formula for the Dice coefficient is the same as that for F1-Score, described as the harmonic mean between Precision and Sensitivity, combining the results of these metrics. Specificity signifies the proportion of areas forecasted by the model as non-interest regions to the actual non-interest regions labeled, measuring the ability to judge pixels in non-interest regions. Accuracy denotes the proportion of areas forecasted by the model as interest regions to all areas.

3.3 Image Enhancement Results and Analysis

This paper analyzes the proposed molybdenum target image enhancement algorithm based on gradient information and contrast reconstruction from subjective visual effects and objective evaluation indicators to comprehensively evaluate it. Fig. 3 shows the results under different enhancement operations. Fig. 3(a) is the original image, and Fig. 3(b) is the image reconstructed based on gradient information, where the boundary gradient of the mass is more significant, to some extent overcoming the problem caused by the gradual edge transition characteristics of breast lesions. Fig. 3(c) is the image reconstructed based on contrast, where the contrast between the mass area and the surrounding environment is significantly improved compared to Fig. 3(a) and Fig. 3(b). Figs. 3(d) and 3(e) are images processed by methods from references [33] and [34] respectively. Fig. 3(d) still does not improve the gradual edge transition characteristics, with unclear gradient information. Although Fig. 3(e) enhances the contrast, it does not highlight the gradient information of the edges. Fig. 3(f) shows the image processed using the technique suggested in this work, which first reconstructs the gradient information and then reconstructs the contrast. This method has more obvious gradient information and dramatically improves the contrast.

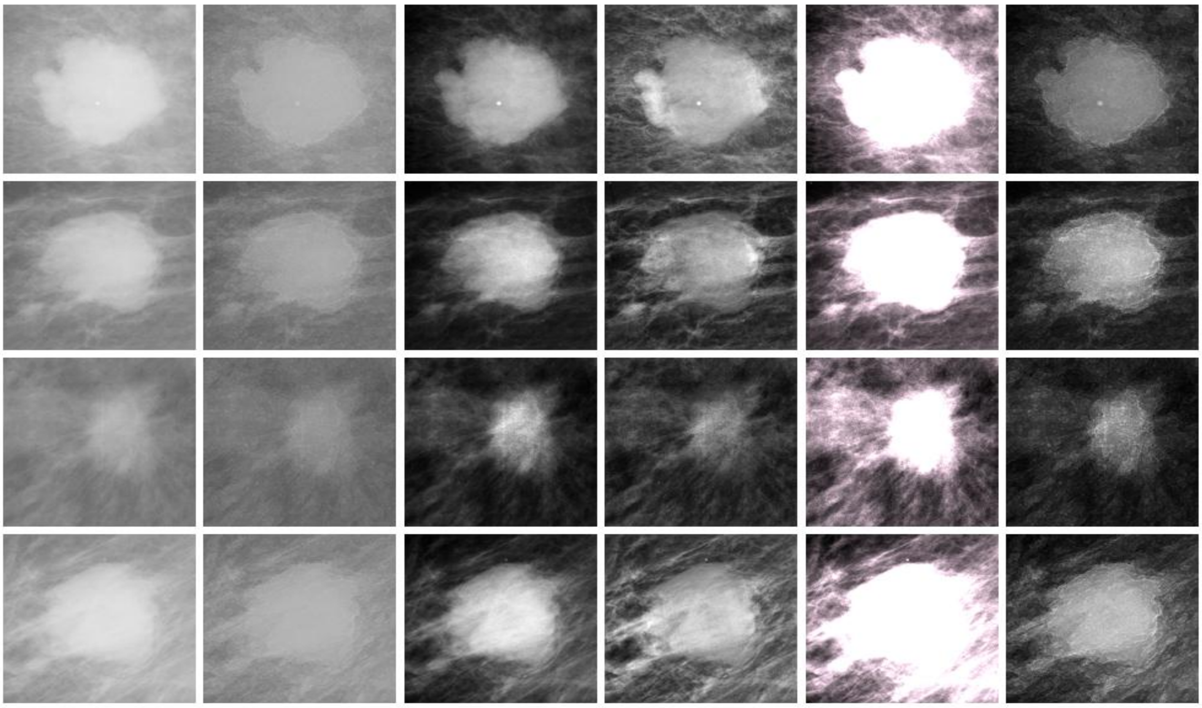

(a) Original image (b) Gradient information reconstruction (c) Contrast reconstruction (d) Reference [33] (e) Reference [34] (f) Proposed method

Figure 3: Images under different enhancement operations

Table 2 shows the objective evaluation indicators of three tumor image samples after different enhancement operations. Using the method proposed in this article, the SF and AG indicators of the images processed by the image enhancement algorithm, which includes gradient information reconstruction and contrast reconstruction, are higher than in other cases. This indicates that the edge information of the breast molybdenum target image after processing with the method proposed in this article is more prominent and more transparent.

Alongside advancements in low-level image quality measurements (SF and AG), it is essential to evaluate the effect of the enhancement procedure on segmentation performance. Consequently, an additional study was performed utilizing the U-Net++ network on datasets enhanced by various ways, and the segmentation outcomes were evaluated. Table 2 demonstrates that the dataset augmented by the suggested method attained a Dice coefficient of 96.52%, an IoU of 93.30%, a sensitivity of 96.56%, and an accuracy of 98.84%, surpassing datasets processed solely using gradient or contrast reconstruction, or lacking augmentation. This verifies that the suggested gradient and contrast enhancement method enhances image clarity and substantially increases U-Net++ segmentation accuracy and boundary precision.

Table 2: Comparison of image enhancement evaluation indexes

Sample	Unenhanced		Gradient information reconstruction		Contrast reconstruction		Proposed method	
	SF	AG	SF	AG	SF	AG	SF	AG
1	4.48	2.69	7.40	4.26	8.81	5.32	15.25	8.71
2	5.52	3.35	9.19	5.33	9.96	5.65	20.21	11.14
3	5.09	3.04	9.28	5.31	11.41	6.83	24.47	13.89

Table 3 delineates the segmentation performance of U-Net++ utilizing various input kinds. Both gradient and contrast reconstructions independently enhance Dice, IoU, sensitivity, and accuracy compared to the original pictures, however, the fully upgraded images attain superior performance across all measures. The results validate that the suggested improvement technique not only elevates image quality but also markedly enhances segmentation efficacy.

Table 3: Impact of Image Enhancement on U-Net++ Segmentation Performance

Input Type	Dice (%)	IoU (%)	Sensitivity (%)	Accuracy (%)
Original Images	94.29	89.36	94.89	98.24
Gradient-Reconstructed Images	95.06	90.64	94.62	98.44
Contrast-Reconstructed Images	95.86	92.11	96.04	98.63
Proposed Method (Full)	96.52	93.30	96.56	98.84

To confirm the superiority of the approach introduced in this study, two excellent domestic and foreign studies of the same kind were selected for comparison. Table 4 compares the suggested technique in this work with the techniques in references [33] and [34] concerning objective evaluation indicators for image enhancement and timeliness. It can be seen that the SF and AG indicators of the images processed by the introduced approach in this study are higher than the other two methods, indicating that the suggested approach in this work has certain advantages in comparison with similar domestic and foreign studies.

Table 4: Comparison of evaluation indexes between the suggested approach and similar studies

Method	SF	AG	Time（s）
Reference[33]	12.85	7.10	7.65
Reference[34]	16.02	8.15	72003.25
Proposed method	16.16	8.23	2271.83

*The bolded parts indicate the best results in this experiment.

The timeliness of the three methods was evaluated to more comprehensively and precisely present the usefulness of the suggested approach. Due to the limited number of samples in the DDSM-BCRP subset, this experiment first processed 60 samples before data augmentation. Therefore, the time required to process 60 images using three image enhancement methods is compared. As demonstrated in Table 4, the introduced approach in this work is superior to reference [34] in both timeliness and image enhancement evaluation indicators. Although the introduced technique in this study is inferior to the technique in reference [33] in terms of timeliness, it outperforms that method regarding image enhancement evaluation indicators.

3.4 Image Segmentation Results and Analysis

3.4.1 Comparison of segmentation results under different enhancement operations

Fig. 4 presents the SRs of the U-Net++ network. Fig. 4(a) shows four samples containing breast masses, while Figs. 4(b), 4(c), 4(d), 4(e), 4(f), and 4(g) demonstrate the predicted SRs from the U-Net++ network for the original images of these four samples, the images reconstructed from gradient information, the images reconstructed from contrast, the results from reference [33], the results from reference [34], and the outcomes processed by the approach suggested in this work, respectively. Fig. 4(h) presents the segmentation outcomes achieved by the suggested methodology, alongside samples depicted in Fig. 4(a) and comparative results illustrated in Figs. 4(b) to 4(g). The proposed method combines gradient and contrast enhancements with U-Net++, resulting in enhanced boundary preservation and mass localization relative to baseline techniques, alongside diminished noise and improved structural detail reconstruction.

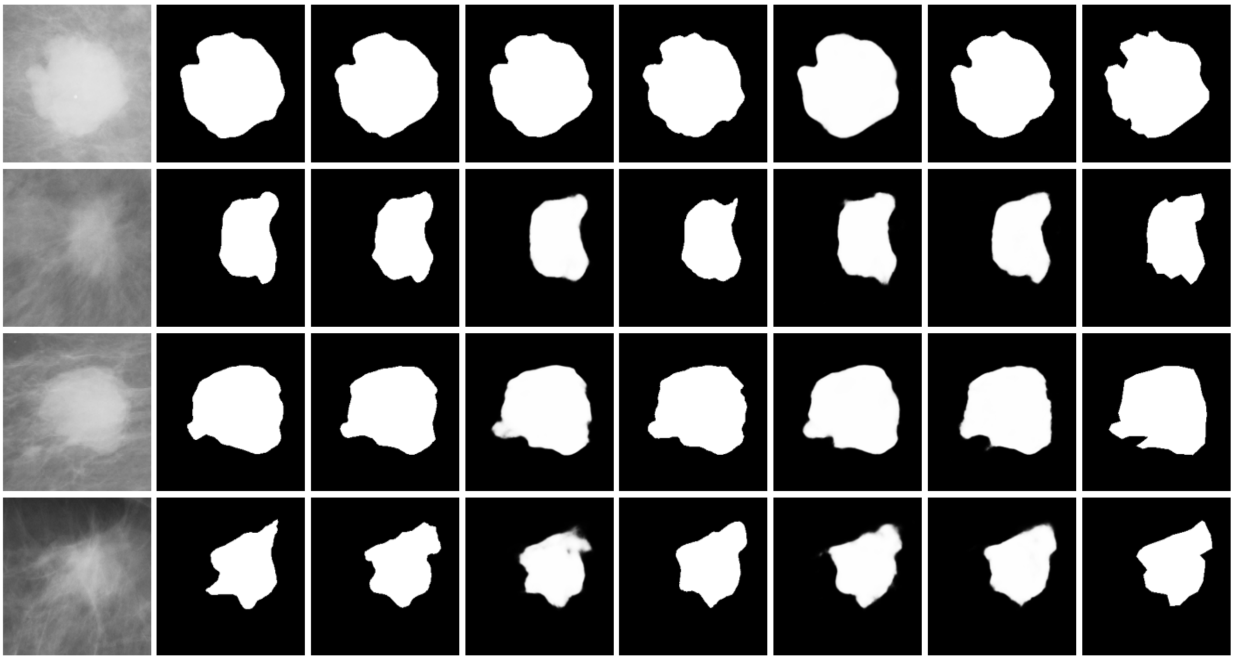

(a) sample (b) Original image (c) Gradient information reconstruction (d) Contrast reconstruction (e) Reference [33] (f) Reference [34] (g) Proposed method (h) label

Figure 4: Comparison of U-Net++ network SRs

To make the SRs more intuitive, the network SRs are outlined with closed curves, as demonstrated in Fig. 5. The area inside the red curve denotes the labeled region, the area inside the white curve signifies the SR after inputting the unenhanced image into the U-Net++ network, the area inside the blue curve denotes the SR after inputting the image reconstructed from gradient information into the U-Net++ network, the area inside the green curve signifies the SR after inputting the image reconstructed from contrast into the U-Net++ network, the area inside the yellow curve denotes the SR after inputting the image processed using the method from reference [33] into the U-Net++ network, the area inside the cyan curve represents the SR after inputting the image processed using the method from the reference [34] into the U-Net++ network, and the area inside the black curve represents the SR after inputting the image processed using the strategy put forth into the U-Net++ network. Fig. 5 juxtaposes the segmentation contours derived from six methodologies superimposed over the original mammograms. (a) illustrates U-Net++ applied to original photos, revealing several boundary irregularities. (b) and (c) present outcomes utilizing gradient- and contrast-enhanced inputs, which promote localization but overlook fine structures. Methods (d) and (e) from references [33] and [34] exhibit intermediate performance, with discrepancies in low-contrast regions. (f) introduces the suggested methodology, which integrates gradient and contrast reconstruction, resulting in enhanced boundary precision and a high degree of correspondence with the ground truth.

Fig. 5(g) presents the segmentation contour lines of the approach suggested in this document, as well as those from references [33] and [34], on a single background.

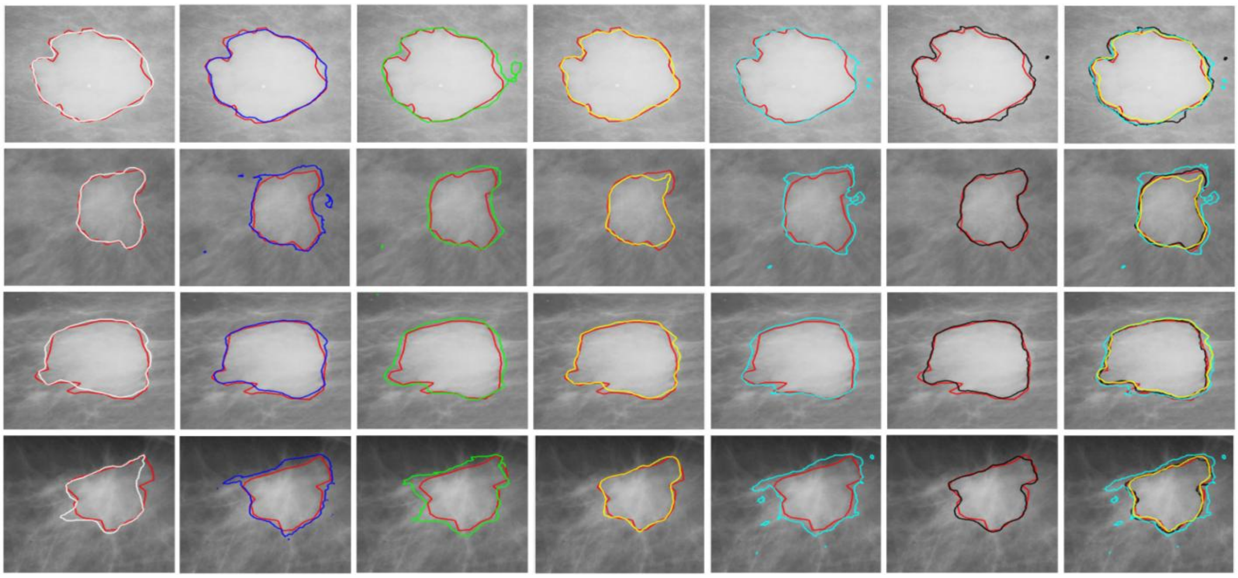

(a)Unenhanced (b) Gradient information reconstruction (c) Contrast reconstruction (d)Reference [33] (e)Reference [34] (f)Proposed method (g)contrast

Figure 5: Comparison of contour lines of U-Net++ network SRs

Through Figs. 4 and 5, it can be visually observed that the segmentation performance of the unenhanced images as the dataset input into the network is unsatisfactory, with the problem of inaccurate edge positioning still quite evident. The SRs of images reconstructed from gradient information as the dataset can better consider edge information and perform well in edge detail recognition. However, the fitting between the segmentation and labeled areas is average. The images reconstructed from contrast as the dataset can better identify the labeled area but perform poorly in recognizing edge detail information.

In the instances depicted in Fig. 5, the segmentation outcomes on the original photos yielded an average Dice score of 94.29%, whereas gradient-reconstructed and contrast-reconstructed inputs enhanced the Dice scores to 95.06% and 95.86%, respectively. The fully upgraded images achieved the highest Dice score of 96.52%, validating that the visual enhancements corresponded with improvements in quantitative segmentation ability.

The overall segmentation performance after processing with the method from reference [33] is good, but compared with the strategy in this work, some SRs have poor edge fitting. The SRs, after processing with the method from the reference [34], have poor fitting between the segmentation area and the labeled area. From Fig. 5(g), it is evident that the black contour line representing the approach suggested in this work fits the red contour line representing the label the best. Therefore, the strategy put forth in this work achieves better outcomes by having a higher distinction in identifying the boundaries of the mass while fully recognizing the labeled area of the mass. Table 5 compares objective evaluation metrics for the segmentation of the U-Net++ network. The image enhancement algorithm in this work, including the reconstruction of gradient information and contrast, outperforms other cases in commonly used pixel-level objective evaluation metrics for MIS.

Table 5: Comparison of segmentation metrics in U-Net++ for the four cases of datasets

Methods	Gradient information reconstruction	Contrast reconstruction	IoU	Precision	Sensitivity	Dice	Specificity	Accuracy
Unenhanced			89.36±0.052	93.98±0.054	94.89±0.030	94.29±0.032	98.89±0.007	98.24±0.009
1	√		90.64±0.045	95.42±0.046	94.62±0.033	95.06±0.027	98.91±0.008	98.44±0.010
2		√	92.11±0.029	95.77±0.026	96.04±0.024	95.86±0.016	99.11±0.007	98.63±0.008
3	√	√	93.30±0.023	96.53±0.020	96.56±0.018	96.52±0.013	99.27±0.005	98.84±0.007

*The bolded parts indicate the optimal outcomes in this test.

To confirm the strategy's advantage concerning segmentation performance, Table 6 provides a comparison of objective evaluation metrics for image segmentation among the U-Net++ network combined with the approach suggested in this document, the method from reference [34], and the method from reference [35]. It can be seen that the image enhancement algorithm put forth in this work, including the reconstruction of gradient information and contrast, outperforms the other two methods in commonly used pixel-level objective evaluation metrics for MIS.

Table 6: Comparison of the suggested technique with similar domestic and foreign studies on the segmentation average index

Methods	IoU	Precision	Sensitivity	Dice	Specificity	Accuracy
Reference**Error! Reference source not found.**	91.72±0.031	95.66±0.029	95.74±0.025	95.65±0.017	99.11±0.006	98.55±0.009
Reference**Error! Reference source not found.**	92.72±0.027	96.36±0.026	96.11±0.020	96.20±0.015	99.18±0.008	98.71±0.009
Proposed method	93.30±0.023	96.53±0.020	96.56±0.018	96.52±0.013	99.27±0.005	98.84±0.007

*The bolded parts indicate the best results in this experiment. To evaluate the reliability of the data, we calculated the mean and standard deviation for each assessment measure over the test folds. Paired t-tests demonstrated statistically substantial enhancements ($p < 0.05$) in Dice and IoU scores when contrasting the suggested strategy with baseline enhancement techniques. The variance in segmentation results was especially pronounced in instances involving small or irregularly shaped masses, or when such masses were situated adjacent to thick glandular tissues. The outlier cases resulted in marginally reduced metric values, underscoring the necessity for more refining in boundary-sensitive situations. To effectively demonstrate the efficacy of the proposed enhancement technique, comparative segmentation outputs are now displayed with uniform labeling across all visual figures. Each figure contains comprehensive captions specifying the input type, segmentation technique, and significant visual observations to enhance clarity and reader understanding. A new summary table has been incorporated to present class-wise segmentation parameters, including Dice coefficient, Intersection over Union (IoU), sensitivity, and specificity, each with 95% confidence intervals. This enhancement facilitates a more comprehensive assessment of the model's efficacy across various lesion types and reinforces the statistical significance and diversity of the findings.

3.4.2 Comparison of segmentation results from different networks

After processing the dataset with the strategy in this work, the data was also fed into the U-Net network for comparison with the SRs of the U-Net++ network. The U-Net++ network is an improvement based on the U-Net, with a more flexible feature fusion method and lower training time cost. The comparison of SRs is demonstrated in Fig. 6. Fig. 6(a) demonstrates four images containing breast mass samples processed by the enhancement algorithm proposed in this paper. Fig. 6(b) shows the corresponding label images of the samples. In contrast, Figs. 6(c) and 6(d) show the SRs in U-Net and U-Net++, respectively. In Fig. 6(e), the area within the red curve signifies the label, the white curve represents the SR of the U-Net network, and the area within the black curve represents the SR of the U-Net++ network.

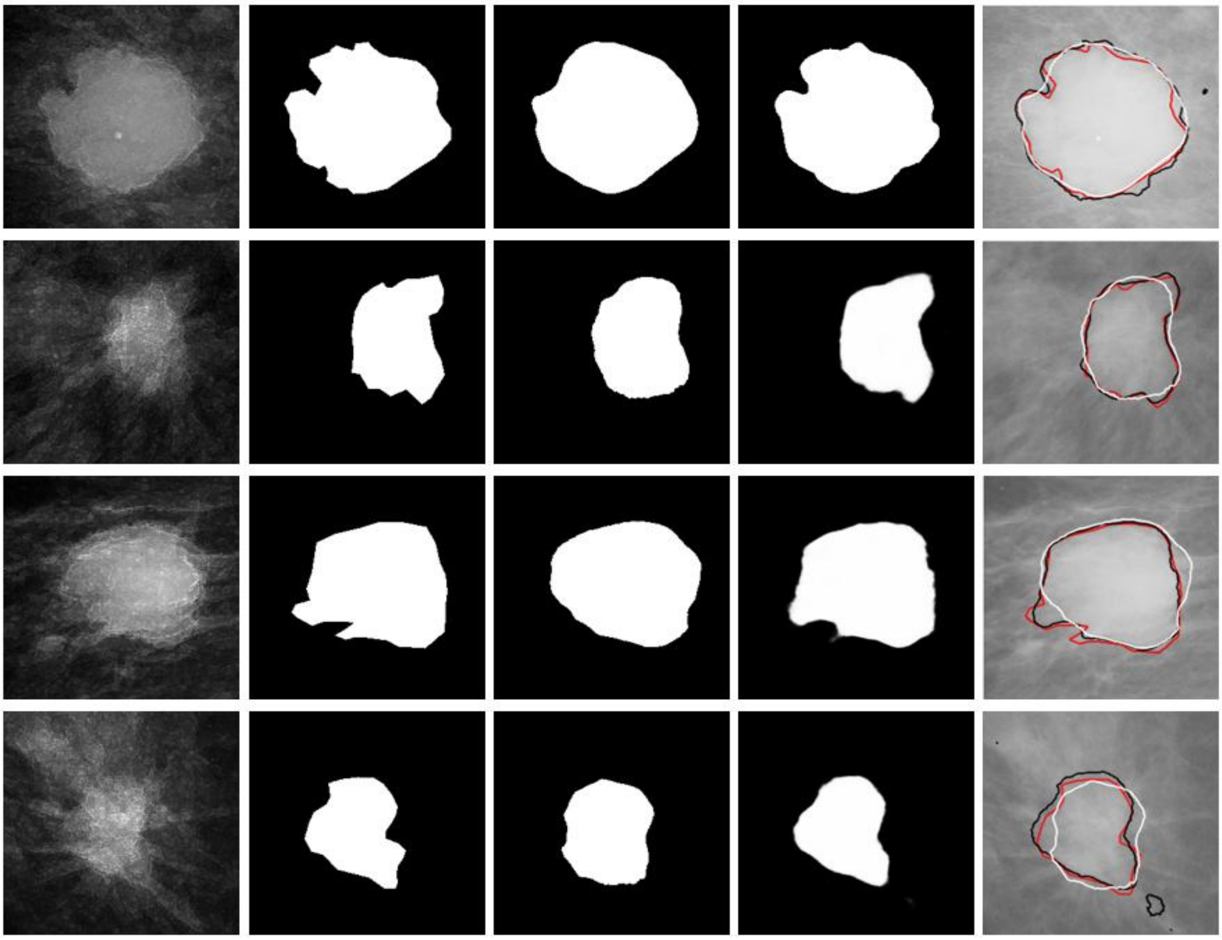

Figure 6: Comparison of different network SRs

Through Fig. 6(c) and Fig. 6(d), it is visually observed that compared to the SRs forecasted by the U-Net++ network model, the SRs forecasted by the U-Net network model have poorer recognition of the edge details of the mass cannot fit the contour of the mass well, and fail to obtain practical segmentation areas. Fig. 6(e) more intuitively reflects the fitting degree of the SRs, with the fitting degree of the black curve and the red curve much higher than that of the white and red curves. Therefore, the segmentation performance of the U-Net++ network is superior to that of the U-Net network.

Table 7 presents the evaluation metrics of U-Net and the approach suggested in this work (U-Net++) under the image enhancement algorithm proposed in this paper. The approach's segmentation performance has been notably boosted in comparison with the U-Net network model.

Table 7: Comparison of segmentation evaluation metrics of the enhancement algorithm suggested in this study on different models

	IoU	Precision	Sensitivity	Dice	Specificity	Accuracy
Proposed enhancement method+U-Net	66.35	74.09	89.20	77.91	93.16	92.21
Proposed method	93.30	96.53	96.56	96.52	99.27	98.84

*The bolded parts indicate the optimal outcomes in this test.

Table 8 provides the segmentation evaluation metrics of breast molybdenum target images for different network models, including U-Net, FCN with attention mechanism and dense connections, U-Net mixed with the enhancement algorithm suggested in this work, end-to-end network model, U-Net++, and U-Net++ combined with the enhancement algorithm proposed in this study. The evaluation metrics incorporate specificity, sensitivity, Dice coefficient, and accuracy.

Table 8: Comparison of evaluation indexes under various network models

Method	Sensitivity	Dice	Specificity	Accuracy

Reference**Error! Reference source not found.**	77.89	82.24	84.69	78.38
Proposed enhancement method+U-Net	89.20	77.91	93.16	92.21
Reference**Error! Reference source not found.**	80.30	85.08	99.76	98.91
U-Net++	94.89	94.29	98.89	98.24
Proposed method	96.56	96.52	99.27	98.84

*The bolded parts show the optimal results in this test.

Table 8 shows that the Dice coefficient and sensitivity, the segmentation performance of feeding the dataset processed by the image enhancement algorithm proposed in this paper, which includes gradient information reconstruction and contrast reconstruction, into the U-Net++ network is superior to additional network structures. However, regarding specificity and accuracy, the method introduced in this document is slightly inferior to the end-to-end network suggested in the reference [36]. Still, the difference is minimal, with a margin of 0.49 % points and 0.07 % points, respectively. However, the sensitivity and Dice coefficient are much higher than the end-to-end network, with margins of 16.26 percentage points and 11.44 percentage points, respectively.

These applications described in this article target the segmentation of masses in the breast on mammograms, which will boost the precision and dependability of CAD systems in medical images. The proposed image-enhancing algorithm, considering both gradient and contrast reconstruction, may be used as a preprocessing method for the mammographic pictures so that the boundary of lesions could be heightened and interference from noise could be reduced. It can be easily implemented in clinical practice to enable radiologists to obtain accurate segmentations of breast masses using up-to-date DL models, namely U-Net++. Moreover, its efficiency, tested with a five-fold cross-validation, facilitates straightforward generalization on other medical image data, including lung nodules and brain tumors. Critical limitations include the fact that this approach is based on a small dataset, the poor adaptiveness of significant and diverse populations, and the different situations in image acquisition that could be foreseen. Regarding computational complexity, high-performance hardware may be required in the enhancement and segmentation process. Limitations that future work may want to deal with include investigating ways of data augmentation and algorithm optimization for real-time and scalable deployment. In addition to segmentation performance, the proposed enhancement and segmentation pipeline needed an average CPU execution time of 0.011325 seconds per image. Memory utilization throughout model inference remained below 1.2 GB, suggesting that the technique is computationally efficient and suited for real-time or clinical application. To assess the contribution of each enhancement component, we performed an ablation study. Using gradient-only input improved Dice from 94.29% to 95.06%, and contrast-only inputs yielded 95.86%. When combined, the proposed method achieved 96.52%, confirming the complementary benefits of both enhancements.

3.5 Discussion

The suggested method was assessed in comparison to other state-of-the-art (SOTA) techniques, including ACA-ATRUNet [17], CNN-based classifiers [19], and enhancement-driven U-Net variations [25]. In comparison to existing models, our improved U-Net++ architecture attained superior segmentation performance across all critical parameters, including Dice (96.52%), IoU (93.30%), and Sensitivity (96.56%). The improvements can be ascribed to two main innovations: (1) the reconstruction of gradient and contrast information before segmentation, enhancing edge clarity and mass delineation, and (2) the linear fusion of structural and edge information, which more effectively maintained lesion boundaries compared to raw input or contrast-only preprocessing.

In contrast to existing methods that depend exclusively on raw pictures or generic denoising techniques, our approach specifically targets the distinct attributes of mammograms, including low contrast and glandular tissue interference, by amplifying low-frequency features and refining edge gradients.

Nonetheless, several segmentation inaccuracies were still noted, especially in instances involving small, irregularly shaped masses or those situated near dense glandular structures. In some instances, the gradient transitions were less distinct, and the adjacent textures occasionally perplexed the model. These problems indicate that the integration of shape priors or adaptive attention techniques may enhance performance in subsequent iterations.

4 Conclusion

This paper focuses on the subjects introduced in the segmentation and analysis by the gradual edge transitions of masses and low contrast in breast mammography images. This study researched several typical segmentation networks in performance by DL integrated with CAD and evaluated different preprocessing methods for their impact on the SR. The significant contribution of the paper is that it proposes an image enhancement algorithm that combines the reconstruction of gradient information with contrast reconstruction to improve the clarity and boundary definition of masses while suppressing noise interference.

Compared with state-of-the-art works at home and abroad through large-scale experiments, the proposed algorithm exhibited significant improvements in segmentation performance, outperforming the existing algorithms in accuracy, sensitivity, and Dice coefficient. Such improvement indicates that the preprocessing enhancement has much potential to boost DL networks for medical image analysis. Future studies will concentrate on the following two significant tasks: maximization of the limited medical image datasets through specific strategies, namely data augmentation and transfer learning, and further enhancing the proposed algorithm's generalization ability for other medical imaging using more datasets, namely lung nodules and brain tumors. Various directions are realized in clinical practice by optimizing the computation efficiency and checking its applicability on more practical and prevalent CAD systems. This could allow further adjustment according to the collaborating radiologists and clinicians' practical clinical experience to refine the operation of the suggested strategy in actual healthcare practice.

The changes not only enhanced the visual clarity of mammographic pictures but also resulted in a quantifiable increase in segmentation accuracy, with the Dice coefficient attaining 96.52% and IoU 93.30% utilizing the U-Net++ model. This study concentrated on breast mass segmentation; however, the methodology rooted in structural preservation and edge enhancement may apply to other areas in medical imaging, including brain tumor segmentation in MRI and lung nodule detection in CT scans. Future research will investigate its adaptability and generalizability across many imaging modalities and datasets.

Nomenclature

Abbreviations	
ACA-AMDN	Attention-Constrained Adaptive-Multidimensional Network
ACA-ATRUNet	Attention-Constrained Adaptive Atrous U-Net
AUC	Area Under the Curve
Bi-ConvLSTM	Bidirectional Convolutional Long Short-Term Memory
BUSI	Breast Ultrasound Images
CAD	Computer-Aided Diagnosis
CLAHE	Contrast Limited Adaptive Histogram Equalization
CNN	Convolutional Neural Network
DDSM	Digital Database for Screening Mammography
EME	Enhancement Measure Estimation
FCN	Fully Convolutional Network
IoU	Intersection over Union
K-SVD	K-Singular Value Decomposition
MIAS	Mammographic Image Analysis Society
MML-EOO	Multi-Model Learning Optimization for Enhanced Output Optimization
PCA	Principal Component Analysis
ROI	Region of Interest
SVM	Support Vector Machine
UDIA	Ultrasonography Dataset for Imaging and Analysis
USM	Unsharp Masking
BCRP	Breast Cancer Resistance Protein
WU-Net++	Weighted U-Net++ model
symbol	
AG	Average Gradient
CF	Column Frequency
D	Dictionary matrix
$F1$	The harmonic means of Precision and Sensitivity
FN	False Negatives
FP	False Positives
H	the total variation of the structural component
I	the input image
K	the inherent variation
L	Sparsity constraint parameter
M	Height (number of rows) of the image
N	Width (number of columns) of the image.
RF	Row Frequency
SF	Spatial Frequency
TN	True Negatives
TP	True Positives
X	Encoding vector
Y	Matrix of given samples
Subscripts	
p	Index of a pixel in the 2D image
q	Index of a pixel within a square region
x	directions of the pixels
y	directions of the pixels
Greek symbol	
γ	grayscale levels

Acknowledgment

The Henan Provincial Science and Technology Research Project funded this work (Grant No. 242102210002). Healthcare Innovation Leading Program at Zhengzhou Science and Technology (Grant No. 2024YLZDJH026). Henan Province Postdoctoral Research Project (001701004), Henan Provincial Youth Science Foundation Project (212300410291), Henan Province Science and Technology Research Project (222102210073), and the National Natural Science Foundation of China Joint Fund Project (U21B2037).

Competing Interests

No competing interests are disclosed by the authors.

Authorship Contribution Statement

Miao GUO: Supervision, Writing-Original draft preparation, Conceptualization, Project administration.
Ating YANG: Methodology, Software
Min DONG: Language review

Data Availability

The authors will provide unrestricted access to the raw data that was used to support this article's conclusions.

Declarations

Not applicable.

Conflicts of Interest

The scholars claimed no conflicts of interest considering this investigation."

Author Statement

All of the writers have read and approved the manuscript. Each author feels that it is honest and that the authorship requirements have been fulfilled, as previously mentioned in this document.

Funding

Not applicable.

Ethical Approval

No research involving humans or animals is included in this investigation.

References

[1] Zahoor, S., I.U. Lali, M.A. Khan, K. Javed and W. Mehmood (2020). Breast cancer detection and classification using traditional computer vision techniques: a comprehensive review. *Current Medical Imaging*, Bentham Science, 16(10), pp. 1187–1200. https://doi.org/10.2174/157340561666620040610547.

[2] Oza, P., U. Oza, R. Oza, P. Sharma, S. Patel, P. Kumar and B. Gohel (2024). Digital mammography dataset for breast cancer diagnosis research (DMID) with breast mass segmentation analysis. *Biomedical Engineering Letters*, Springer Nature, 14(2), pp. 317–330. https://doi.org/10.1007/s13534-023-00339-y.

[3] Roy, S., D. Das, S. Lal and J. Kini (2023). Novel edge detection method for nuclei segmentation of liver cancer histopathology images. *Journal of Ambient Intelligence and Humanized Computing*, Springer Nature, 14(1), pp. 479–496. https://doi.org/10.1007/s12652-021-03308-4.

[4] Javadpour, A. and A. Mohammadi (2016). Improving brain magnetic resonance image (MRI) segmentation via a novel algorithm based on genetic and regional growth. *Journal of Biomedical Physics & Engineering*, Shiraz University of Medical Sciences, 6(2), pp. 95. https://pmc.ncbi.nlm.nih.gov/articles/PMC5022759/.

[5] XU, J., T. ZHAO, G. FENG and S. OU (2021). Image Segmentation Algorithm Based on Context Fuzzy C-Means Clustering. *电子与信息学报*, Aerospace Information Research Institute, Chinese Academy of Sciences, 43(7), pp. 2079–2086. http://dx.doi.org/10.11999/JEIT200263.

[6] WANG, X., Q. WANG, J. JIAO and J. LIANG (2021). Fuzzy C-means clustering with fast and adaptive non-local spatial constraint and membership linking for noise image segmentation. *电子与信息学报*, Aerospace Information Research Institute, Chinese Academy of Sciences, 43(1), pp. 171–178. https://doi.org/10.11999/JEIT191016.

[7] Fijri, A.L. and Z. Rustam (2018). Comparison between fuzzy kernel c-means and sparse learning fuzzy c-means for breast cancer clustering, In *2018 International Conference on Applied Information Technology and Innovation (ICAITI)*, IEEE, Padang, Indonesia, pp. 158–161. https://doi.org/10.1109/ICAITI.2018.8686707.

[8] Siddique, N., S. Paheding, C.P. Elkin and V. Devabhaktuni (2021). U-net and its variants for medical image segmentation: A review of theory and applications. *IEEE Access*, IEEE, 9, pp. 82031–82057. https://doi.org/10.1109/ACCESS.2021.3086020.

[9] LUO, H., F. LU and F. KONG (2019). Image semantic segmentation based on region and deep residual network. *电子与信息学报*, Aerospace Information Research Institute, Chinese Academy of Sciences, 41(11), pp. 2777–2786. https://doi.org/10.11999/JEIT190056.

[10] YANG, H. and F. WANG (2019). Meteorological radar noise image semantic segmentation method based on deep convolutional neural network. *电子与信息学报*, Aerospace Information Research Institute, Chinese Academy of Sciences, 41(10), pp. 2373–2381. https://doi.org/10.11999/JEIT190098.

[11] de Oliveira, C.E.G., S.L. Vieira, C.F.B. Paranaiba and E.N. Itikawa (2025). Breast tumor segmentation in ultrasound images: comparing U-net and U-net++. *Research on Biomedical Engineering*, Springer Nature, 41(1), pp. 1–11.

[12] Wisaeng, K (2023). U-Net++ DSM: improved U-Net++ for brain tumor segmentation with deep supervision mechanism. *IEEE Access*, 11, pp. 132268–132285. https://doi.org/10.1007/s42600-025-00402-w.

[13] Tiryaki, V.M (2023). Mass segmentation and classification from film mammograms using cascaded deep transfer learning. *Biomedical Signal Processing and Control*, Elsevier, 84, pp. 104819. https://doi.org/10.1016/j.bspc.2023.104819.

[14] Ronneberger, O., P. Fischer and T. Brox (2015). U-net: Convolutional networks for biomedical image segmentation, In *Medical Image Computing and Computer-Assisted Intervention–MICCAI 2015: 18th International Conference, Munich, Germany, October 5-9, 2015, Proceedings, Part III 18*, Springer, Cham, Germany, pp. 234–241. https://doi.org/10.1007/978-3-319-24574-4_28.

[15] Ma, Z., Y. Qi, C. Xu, W. Zhao, M. Lou, Y. Wang and Y. Ma (2023). ATFE-Net: Axial Transformer and Feature Enhancement-based CNN for ultrasound breast mass segmentation. *Computers in Biology and Medicine*, Elsevier, 153, pp. 106533. https://doi.org/10.1016/j.compbiomed.2022.106533.

[16] Malekmohammadi, A., M. Soryani and E. Kozegar (2024). Mass segmentation in automated breast ultrasound using an enhanced attentive UNet. *Expert Systems with Applications*, Elsevier, 245, pp. 123095. https://doi.org/10.1016/j.eswa.2023.123095.

[17] Yaqub, M., F. Jinchao, N. Aijaz, S. Ahmed, A. Mehmood, H. Jiang and L. He (2024). Intelligent breast cancer diagnosis with two-stage using mammogram images. *Scientific Reports*, Springer Nature, 14(1), pp. 16672. https://doi.org/10.1038/s41598-024-65926-0.

[18] Rahman, H., T.F. Naik Bukht, R. Ahmad, A. Almadhor and A.R. Javed (2023). Efficient breast cancer diagnosis from complex mammographic images using deep convolutional neural network. *Computational Intelligence and Neuroscience*, Wiley Online Library, 2023(1), pp. 7717712. https://doi.org/10.1155/2023/7717712.

[19] Mahmood, T., J. Li, Y. Pei, F. Akhtar, M.U. Rehman and S.H. Wasti (2022). Breast lesions classifications of mammographic images using a deep convolutional neural network-based approach. *Plos One*, PLOS, 17(1), p. e0263126. https://doi.org/10.1371/journal.pone.0263126.

[20] Almalki, Y.E., T.A. Soomro, M. Irfan, S.K. Alduraibi and A. Ali (2022). Impact of image enhancement module for analysis of mammogram images for diagnostics of breast cancer. *Sensors*, MDPI, 22(5), pp. 1868. https://doi.org/10.3390/s22051868.

[21] Avcı, H. and J. Karakaya (2023). A novel medical image enhancement algorithm for breast cancer detection on mammography images using machine learning. *Diagnostics*, MDPI, 13(3), pp. 348. https://doi.org/10.3390/diagnostics13030348.

[22] Aliniya, P., M. Nicolescu, M. Nicolescu and G. Bebis (2024). Improved Loss Function for Mass Segmentation in Mammography Images Using Density and Mass Size. *Journal of Imaging*, MDPI, 10(1), pp. 20. https://doi.org/10.3390/jimaging10010020.

[23] Tiryaki, V.M (2023). Mass segmentation and classification from film mammograms using cascaded deep transfer learning. *Biomedical Signal Processing and Control*, Elsevier, 84, pp. 104819. https://doi.org/10.1016/j.bspc.2023.104819.

[24] Wisaeng, K (2023). U-Net++ DSM: improved U-Net++ for brain tumor segmentation with deep supervision mechanism. *IEEE Access*, IEEE, 11, pp. 132268–132285. https://doi.org/10.1109/ACCESS.2023.3331025.

[25] Das, S., R. Dubey, B. Jena, L.-W. Tsai and S. Saxena (2024). WU-Net++: A novel enhanced Weighted U-Net++ model for brain tumor detection and segmentation from multi-parametric magnetic resonance scans. *Multimedia Tools and Applications*, Springer Nature, 1–24. https://doi.org/10.1007/s11042-024-18336-3.

[26] Tambe-Jagtap, S.N. and Z.A. Jaaz (2023). Integrative Genomic and Proteomic Profiling for Personalized Oncological Treatments: Enhancing Therapeutic Efficacy and Reducing Adverse Effects in Breast Cancer Patients. *SHIFAA*, 2023, pp. 1–9. http://dx.doi.org/10.70470/SHIFAA/2023/001.

[27] El Houby, E.M.F (2025). A Review of Machine Learning Techniques in the Medical Domain. *Informatica*, Slovenian Society Informatika, 49(16). https://doi.org/10.31449/inf.v49i16.6934.

[28] Shangguan, T., C. Yang and Y. Zhang (2025). ICU-Net: A U-shaped Low-Dose CT Image Denoising Network Based on Codec Structure. *Informatica*, Slovenian Society Informatika, 49(6). https://doi.org/10.31449/inf.v49i6.7226.

[29] Chegireddy, R.P.R. and A. Srinagesh (2023). A Novel Method for Human MRI Based Pancreatic Cancer Prediction Using Integration of Harris Hawks Varients & VGG16: A Deep Learning Approach. *Informatica*, Slovenian Society Informatika, 47(1). https://doi.org/10.31449/inf.v47i1.4433.

[30] Xu, L., Q. Yan, Y. Xia and J. Jia (2012). Structure extraction from texture via relative total variation. *ACM Transactions on Graphics (TOG)*, ACM Journals, 31(6), pp. 1–10. https://doi.org/10.1145/2366145.2366158.

[31] Verma, G. and M. Kumar (2022). Systematic review and analysis on underwater image enhancement methods, datasets, and evaluation metrics. *Journal of Electronic Imaging*, SPIE Digital Library, 31(6), pp. 60901. https://doi.org/10.1117/1.JEI.31.6.060901.

[32] Mittal, H., A.C. Pandey, M. Saraswat, S. Kumar, R. Pal and G. Modwel (2022). A comprehensive survey of image segmentation: clustering methods, performance parameters, and benchmark datasets. *Multimedia Tools and Applications*, Springer Nature, 1–26. https://doi.org/10.1007/s11042-021-10594-9.

[33] Du, G., M. Dong, Y. Sun, S. Li, X. Mu, H. Wei, L. Ma and B. Liu (2019). A new method for

detecting architectural distortion in mammograms by NonSubsampled contourlet transform and improved PCNN. *Applied Sciences*, MDPI, 9(22), pp. 4916. https://doi.org/10.3390/app9224916.

[34] Liu, R., L. Ma, J. Zhang, X. Fan and Z. Luo (2021). Retinex-inspired unrolling with cooperative prior architecture search for low-light image enhancement, In *Proceedings of the IEEE/CVF Conference on Computer Vision and Pattern Recognition*, IEEE, Nashville, TN, USA, pp. 10561–10570. https://doi.org/10.1109/CVPR46437.2021.01042.

[35] Li, S., M. Dong, G. Du and X. Mu (2019). Attention dense-u-net for automatic breast mass segmentation in digital mammogram. *IEEE Access*, IEEE, 7, pp. 59037–59047. https://doi.org/10.1109/ACCESS.2019.2914873.

[36] Zhou, L., M. Ding, L. Xu, Y. Zhou and X. Zhang (2019). The Automatic Segmentation of Mammographic Mass Using the End-To-End Convolutional Network Based on Dense-Prediction. *Journal of Medical Imaging and Health Informatics*, Ingenta CONNECT, 9(7), pp. 1429–1434. https://doi.org/10.1166/jmihi.2019.2739.